

Design principles for lymphatic drainage of fluid and solutes from collagen scaffolds

Rebecca L. Thompson,¹ Emily A. Margolis,¹ Tyler J. Ryan,¹ Brent J. Coisman,¹ Gavrielle M. Price,¹ Keith H. K. Wong,¹ Joe Tien^{1,2}

¹Department of Biomedical Engineering, Boston University, 44 Cummington Mall, Boston, Massachusetts 02215

²Division of Materials Science and Engineering, Boston University, 15 St. Mary's Street, Brookline, Massachusetts 02446

Received 19 June 2017; revised 4 August 2017; accepted 24 August 2017

Published online 26 September 2017 in Wiley Online Library (wileyonlinelibrary.com). DOI: 10.1002/jbm.a.36211

Abstract: *In vivo*, tissues are drained of excess fluid and macromolecules by the lymphatic vascular system. How to engineer artificial lymphatics that can provide equivalent drainage in biomaterials remains an open question. This study elucidates design principles for engineered lymphatics, by comparing the rates of removal of fluid and solute through type I collagen gels that contain lymphatic vessels or unseeded channels, or through gels without channels. Surprisingly, no difference was found between the fluid drainage rates for gels that contained vessels or bare channels. Moreover, solute drainage rates were greater in collagen gels that contained lymphatic vessels than in those that had bare channels. The enhancement of solute drainage by lymphatic endothelium was more pronounced in longer scaffolds and with smaller solutes. Whole-scaffold

imaging revealed that endothelialization aided in solute drainage by impeding solute reflux into the gel without hindering solute entry into the vessel lumen. These results were reproduced by computational models of drainage with a flow-dependent endothelial hydraulic conductivity. This study shows that endothelialization of bare channels does not impede the drainage of fluid from collagen gels and can increase the drainage of macromolecules by preventing solute transport back into the scaffold. © 2017 Wiley Periodicals, Inc. *J Biomed Mater Res Part A*: 106A: 106–114, 2018.

Key Words: genipin, lymphoscintigraphy, dextran, endothelial cell, microvascular tissue engineering

How to cite this article: Thompson RL, Margolis EA, Ryan TJ, Coisman BJ, Price GM, Wong KHK, Tien J. 2018. Design principles for lymphatic drainage of fluid and solutes from collagen scaffolds. *J Biomed Mater Res Part A* 2018;106A:106–114.

INTRODUCTION

Nearly all tissues in the human body are drained by specialized structures known as lymphatic vessels.¹ If any part of the lymphatic tree is dysfunctional, then drainage is impaired and a low tissue fluid pressure cannot be maintained.² In tissues that are surrounded by a tight sheath, decreased drainage may reduce blood flow and progress to compartment syndrome.³ In more compliant tissues, impaired drainage may present with swelling (lymphedema), stiffness, and abnormal immune response. Both situations, if severe enough, can result in permanent tissue damage.

The most distal portion of the lymphatics—the initial lymphatics, or lymphatic capillaries—are thin, blind-ended vessels through which excess fluid and solutes enter the lymphatic system from the surrounding tissue.^{4,5} The lack of a proper basement membrane around initial lymphatics is believed to facilitate entry of fluid into the vessel.^{6,7} Likewise, the endothelial cell-cell junctions in initial lymphatics are

organized so that they enhance drainage; the junctions consist of intertwining “buttons,” instead of the continuous “zippers” seen in much of the blood vessel system.⁸ These junctions allow the lymphatic vessel wall to act as a collection of one-way valves, so that fluid can flow easily from the tissue into the lymphatic lumen, but not in the reverse direction.⁹ Flow through initial lymphatics is slow (<1 $\mu\text{L}/\text{hr}$ at baseline),¹⁰ and is driven by external compression and by the rhythmic contraction of lymphatic muscle in downstream collecting lymphatics.^{11,12}

When engineering small or thin (maximum dimension of ~ 1 mm) tissues, explicit consideration of lymphatic drainage appears unnecessary, as excess tissue fluid can escape by percolation through the thickness of the construct. As the size of engineered tissues becomes larger, however, lymphatic drainage will likely become more important. Without explicit features designed to improve drainage, larger tissue constructs will be more susceptible to fluid and solute

Correspondence to: J. Tien; e-mail: jtien@bu.edu

Contract grant sponsor: National Cancer Institute; contract grant number: CA214292

Contract grant sponsor: National Heart, Lung, and Blood Institute; contract grant number: HL092335

Contract grant sponsor: Dean's Catalyst Award, Boston University

Contract grant sponsor: Undergraduate Research Opportunities Program, Boston University

Contract grant sponsor: Clare Boothe Luce Scholarship, Boston University

Contract grant sponsor: Summer Term Alumni Research Scholarship, Boston University

accumulation because their surface area-to-volume ratios are smaller.

Little is known, however, about quantitative design principles that enable artificial lymphatic-like structures to provide functional drainage. For instance, beyond what scaffold size are explicit drainage channels required? Does endothelialization of these channels help or hinder drainage? What advantages, if any, do engineered lymphatic vessels hold over bare channels in terms of drainage? Which properties of the endothelium underlie these differences in drainage? Do these design principles differ when considering fluid versus solute drainage? We have shown that adding bare drainage channels to an engineered tissue can avoid an elevated fluid pressure within the scaffold and thus can help stabilize nearby vasculature mechanically,^{13,14} but it is not known whether such structures enhance fluid and/or solute drainage.

This study addresses many of these open questions, using a model *in vitro* system of drainage through micropatterned collagen gels. In particular, it examines the rates of fluid and solute removal from collagen gels that contained explicit channels for drainage; these channels were left unseeded (as in previous work¹⁴) or were seeded with lymphatic endothelial cells (LECs) to form an artificial vessel.¹⁵ We analyzed the solute drainage rate in a gel by adding fluorescent media to one end of the gel and measuring the rate at which the fluorescent solute escaped through the gel and into the channel under lymphatic-like pressures. Surprisingly, we found that the presence of lymphatic endothelium on the channel not only did not impede drainage when compared with a bare channel but, in some cases, greatly enhanced it.

MATERIALS AND METHODS

Cell culture

Human dermal microvascular LECs (lots 6120704.1, 2011204, and 0070602 from Promocell) were grown on gelatin-coated tissue culture dishes in endothelial cell growth media (ECGM) at 37°C and 5% CO₂. ECGM consisted of MCDB131 media (Caisson) supplemented with 10% heat-inactivated fetal bovine serum (Atlanta Biologicals), 1% glutamine-penicillin-streptomycin (Invitrogen), 1 µg/mL hydrocortisone (Sigma), 2 U/mL heparin (Sigma), 0.2 mM L-ascorbic acid 2-phosphate (Sigma), and 25 µg/mL endothelial cell growth supplement (Biomedical Technologies). Cells were passaged at a 1:4 ratio and discarded after passage 10.

Formation of collagen gels that contain drainage channels

Patterned type I collagen gels [from rat tail (BD Biosciences), ~7 mg/mL final concentration in phosphate-buffered saline (PBS); $n = 101$] were formed at room temperature (22–24°C) around 120-µm-diameter, round-tipped needles in 9-, 19-, or 26-mm-long silicone (PDMS) chambers with a 1×1 mm² cross-section [Fig. 1(A)]. For all samples, the tip of the needle was located 1–1.5 mm from one end of the chamber. After forty minutes of gelation, the needles were removed to form a collagen gel that contained a 1- to 1.5-mm-long solid region adjacent to a 7-, 17-, or 24-mm-long region that contained a

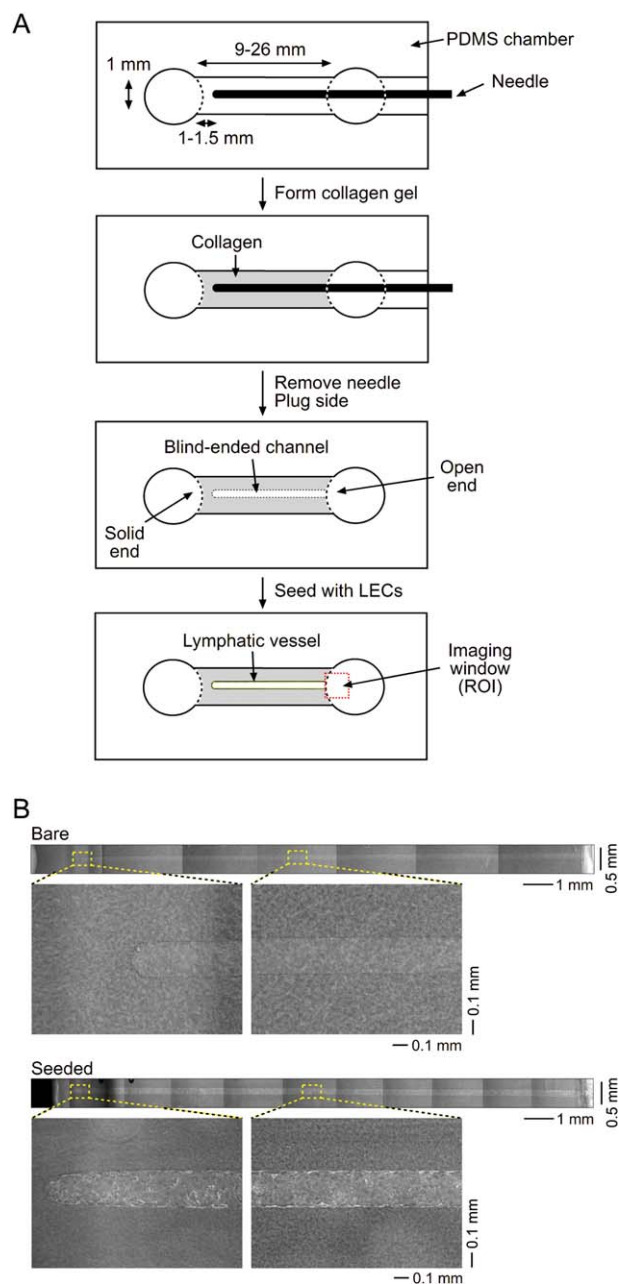


FIGURE 1. Formation of collagen gels that contain blind-ended bare channels or lymphatic vessels. A: Schematic diagram (top view) of experimental procedure. The red dotted rectangle indicates the imaging window used for solute drainage measurements. B: Phase-contrast images of bare channels and endothelialized collagen gels on day 3 post-seeding. Open ends of channels are located at the right sides of stitched images.

bare channel. We used round-tipped needles, which were made by grinding sharp needles (Seirin) gently against a rough surface, to avoid angular features at the tip of the channel that could favor stress concentration and cell detachment.¹⁶

Gels were crosslinked by flushing with 20 mM genipin (Wako Biosciences) in PBS for two hours at room temperature, and were then washed with PBS for at least 12 h to remove residual genipin. Crosslinked gels were conditioned with perfusion media [ECGM supplemented with 3% 70 kDa dextran

(Sigma) and 400 μM dibutyryl cyclic adenosine monophosphate [db-cAMP; Sigma] for at least one day at room temperature. Crosslinking and the addition of dextran and db-cAMP were intended to promote the adhesion of LECs to the channel.¹⁷⁻¹⁹

Solid gels ($n = 29$), that is, gels that did not contain channels, were formed using the same procedure described above, but in the absence of needles.

Formation of blind-ended lymphatic vessels

Conditioned gels were seeded by flowing concentrated LEC suspensions into the channels and allowing the cells to settle and adhere, as described previously.^{15,20} Briefly, the LECs from one confluent 100-mm-diameter dish were pelleted at 100 g for 4 min and resuspended in ~ 40 μL of perfusion media. A small volume (~ 2 μL) of dense cell suspension was then added to the open mouth of the channel and allowed to flow in slowly. Once the cells reached the rounded tip of the channel, the dish was tilted until flow stopped, which allowed cells to settle and adhere to the collagen. Flow was then reversed for ten minutes by adding excess (~ 60 μL) media to the opposite well (that is, the one next to the solid end of the gel), which caused unattached cells to flow out of the channel. The nonadherent cells were removed by rinsing the well next to the open end of the channel with perfusion media several times. After seeding, samples were placed under dropwise forward flow by adding 80 μL of perfusion media to the open end of the channel and 40 μL to the opposite well (equivalent to a pressure difference of 0.1 cm H_2O). All media was replaced twice daily to regenerate the pressure difference. Seeded samples reached confluence and formed blind-ended lymphatic vessels by day 3 after seeding.

Fluid drainage assay

On day 3 after seeding, scaffolds that contained lymphatic vessels or bare channels were placed under a reverse pressure difference of 0.3–0.4 cm H_2O for at least 4 h (i.e., 60 μL of media at the open end and ~ 200 μL at the opposite well). Under these pressure conditions, interstitial flow was directed from the solid end of the gel into the channel and eventually out into the well adjacent to the open end of the vessel or bare channel. The mass of fluid that drained into the well after another 2.5–5 h was removed and weighed. The fluid drainage rate was converted to $\mu\text{L}/\text{h}$ using the density of media. Similar measurements were performed on solid gels.

Solute drainage assay

The drainage assay was modeled after lymphoscintigraphy, a method to evaluate the effectiveness of lymphatics in draining a radiolabeled protein from tissue *in vivo*²¹; we adapted the procedure for use with fluorescent solutes *in vitro*. On day 3 post-seeding, samples were placed under a reverse pressure difference of 0.3–0.4 cm H_2O for at least four hours. Perfusion media that contained 100 $\mu\text{g}/\text{mL}$ Alexa Fluor 488-conjugated dextran (3 or 10 kDa; Invitrogen) and/or Alexa Fluor 594-conjugated bovine serum albumin (BSA;

Invitrogen) or 10 kDa dextran was then added to the well at the solid end of the gel, again under a reverse pressure difference of 0.3–0.4 cm H_2O . The region-of-interest (ROI) at the open end of the lymphatic vessel or bare channel was imaged every 2 min for 88 min with a Plan-Neofluar $5\times/0.15$ objective (Zeiss), beginning immediately after the addition of the fluorescent media. All images were corrected for non-uniformity of illumination using Axiovision ver. 4.5 (Zeiss). Similar time-lapse imaging was performed on solid gels at the end opposite to the one where solute was added. In some cases, the entire scaffold was imaged at the end of the drainage assay, and images were stitched to yield composite views of solute distribution.

Solute drainage rates were calculated by averaging fluorescence intensities over the ROI for each time-point, normalizing the intensities by that of bulk media, and determining the rate at which the normalized fluorescence intensities increased over time:

$$\text{Solute drainage rate} = \frac{I_2 - I_1}{t_2 - t_1} \frac{t_{\text{bulk}}}{t_{\text{sample}}} \frac{1}{I_{\text{bulk}} - I_{\text{bgd}}}$$

where I_1 and I_2 are the average ROI intensities at times t_1 and t_2 , t_{sample} and t_{bulk} are the exposure times used to image the ROI and bulk media, I_{bulk} is the average intensity of bulk media, and I_{bgd} is the average intensity of a solute-free area. Solute drainage rates are reported in units of 1/min; fluorescence intensities are given in arbitrary units.

To determine the sensitivity of this assay, we repeated the measurements and calculations with scaffolds in which fluorescent solutes were not added to the perfusion media.

Measurement of LEC hydraulic conductivity

Solid, 5-mm-long collagen gels (3 mg/mL) were formed in a PDMS chamber, crosslinked with 20 mM genipin for 1.5 h, and flushed with PBS overnight and with media for one day. Gels were then seeded at one end by adding a suspension of LECs to one well and tilting the sample to allow cells to settle onto the gel; seeded gels were held in perfusion media under a forward pressure difference of 0.1 cm H_2O . On the third day after seeding, samples were placed under a reverse pressure difference of up to 1.2 cm H_2O for at least 4 h before measuring the flow rate over 1 h. The endothelium was then removed with a 2-min exposure to media that contained 0.5% Triton X-100, and the flow rate was measured again. The endothelial hydraulic conductivity was calculated by treating the gel and LEC monolayer as two hydraulic resistors in series using Starling's Law of Filtration.²²

Numerical modeling

Finite-element models of fluid and solute transport in collagen gels of different configurations were solved in COMSOL Multiphysics ver. 3.5 (Comsol). Fluid transport through a gel and channel were governed by Darcy's Law and the Navier-Stokes equations, using experimentally determined gel permeabilities. Fluid flow across endothelium was governed by Starling's Law with a pressure-dependent hydraulic conductivity that was obtained from experimental data. Solute transport within a gel

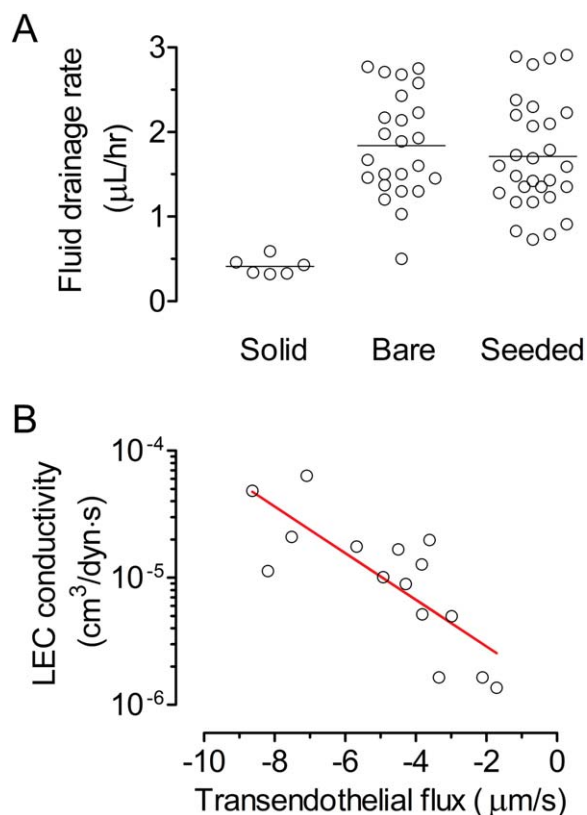


FIGURE 2. Fluid drainage. A: Flow rates through 19-mm-long gels that did or did not contain drainage channels. Channels were either bare or seeded with LECs to form vessels. B: Plot of endothelial hydraulic conductivity versus transmurial (i.e., transendothelial) flow speed. The red line denotes the best log-linear fit to experimental data.

and channel were convective. The ratio of endothelial solute permeability to hydraulic conductivity was assumed to be 1000 dyn/cm^2 for 3 kDa dextran (diffusion coefficient of $130 \mu\text{m}^2/\text{s}$), 500 dyn/cm^2 for 10 kDa dextran ($65 \mu\text{m}^2/\text{s}$), and 350 dyn/cm^2 for BSA ($45 \mu\text{m}^2/\text{s}$).^{23,24} Fluid transport equations for steady flow were solved first, and the resulting flow field was used to solve the unsteady solute transport equations, in which a solute of unit concentration was introduced at time $t = 0 \text{ min}$ to the solid end of the gel. Solute fluxes were integrated over the surface of the gel and channel exit to determine the solute drainage rate at $t = 88 \text{ min}$; similar integrations yielded fluid drainage rates. Meshes were refined until the drainage rates of two sequentially refined models differed by $<1\%$; typical models had 10^5 – 5×10^6 degrees-of-freedom.

Statistical analysis

Statistical analysis was performed with Prism ver. 5 (Graphpad). Pairwise comparisons used the Mann-Whitney U test. Comparisons to the nominal minimum detectable solute drainage rate ($10^{-6}/\text{min}$) used Wilcoxon's signed rank test. We considered a difference to be statistically significant if p was <0.05 divided by the number of comparisons made. For the fluid drainage data in Figure 2, this condition was $p < 0.017$; for the solute drainage data in Figures 4 and 5, it was $p < 0.0015$. Fluid and solute drainage rates are given as

arithmetic means \pm SD and geometric means with 95% CI, respectively. Arithmetic and geometric means are provided in plots of fluid and solute drainage rates, respectively.

RESULTS

Formation of blind-ended lymphatic vessels in patterned collagen gels

LECs began to attach and spread on the walls of the channel in the collagen scaffold within 1 h after seeding. All samples showed large portions of confluent endothelium the day after seeding (day 1), which proliferated to cover nearly the entire channel wall by the second day after seeding (day 2). Phase-contrast images showed that confluent, blind-ended tubes ("vessels") of LECs formed by day 3 [Fig. 1(B)]. We cultured the samples under a forward pressure difference (i.e., with pressure in the lumen greater than pressure in the gel), which should exert a stabilizing transmural pressure.¹⁶ This pressure condition allowed the lymphatic endothelium to remain adherent to the collagen gel; on day 3, we reversed the direction of the pressure gradient for at least 4 h prior to the fluid and solute drainage assays to acclimate the endothelium to lymphatic-like negative transmural pressures.

Fluid drainage through channels is not affected by endothelialization

Under a pressure difference of $\sim 0.4 \text{ cm H}_2\text{O}$, 19-mm-long solid gels displayed fluid drainage rates of $0.41 \pm 0.10 \mu\text{L/h}$ on day 3 [Fig. 2(A)]. Scaffolds that contained bare channels drained fluid at much higher rates than solid gels did ($1.84 \pm 0.62 \mu\text{L/h}$; $p = 0.0003$). Scaffolds that contained lymphatic vessels also drained fluid faster than solid gels did ($1.71 \pm 0.65 \mu\text{L/h}$; $p = 0.0002$). Surprisingly, drainage rates were not affected by endothelialization of channels ($p = 0.42$). These data indicate that the presence of a channel, but not that of an endothelial lining, controlled fluid drainage rates; these data also imply that the endothelium in seeded channels was leaky enough that it did not impede fluid drainage.

To understand why the endothelium did not hinder fluid drainage, we measured the hydraulic conductivity L_P of the lymphatic endothelium under different reverse pressures [Fig. 2(B)]. The data displayed a log-linear dependence of L_P on transmural flow speed J_v :

$$\log L_P = -0.1834 J_v - 5.906$$

with L_P and J_v given in units of $\text{cm}^3/\text{dyn}\cdot\text{s}$ and $\mu\text{m/s}$, respectively. That is, greater fluid absorption corresponded to a more permeable lymphatic endothelium. Since the blind-ended tip of the vessel is where fluid flux is expected to be largest (see "Discussion"), the LEC layer should be leakiest at the vessel tip and thus be less likely to hinder fluid drainage.

Drainage of 10 kDa dextran can be enhanced by endothelialization

To assess the ability of channels with and without endothelium to enhance solute drainage in 19-mm-long collagen gels, we placed samples on day 3 under a reverse pressure

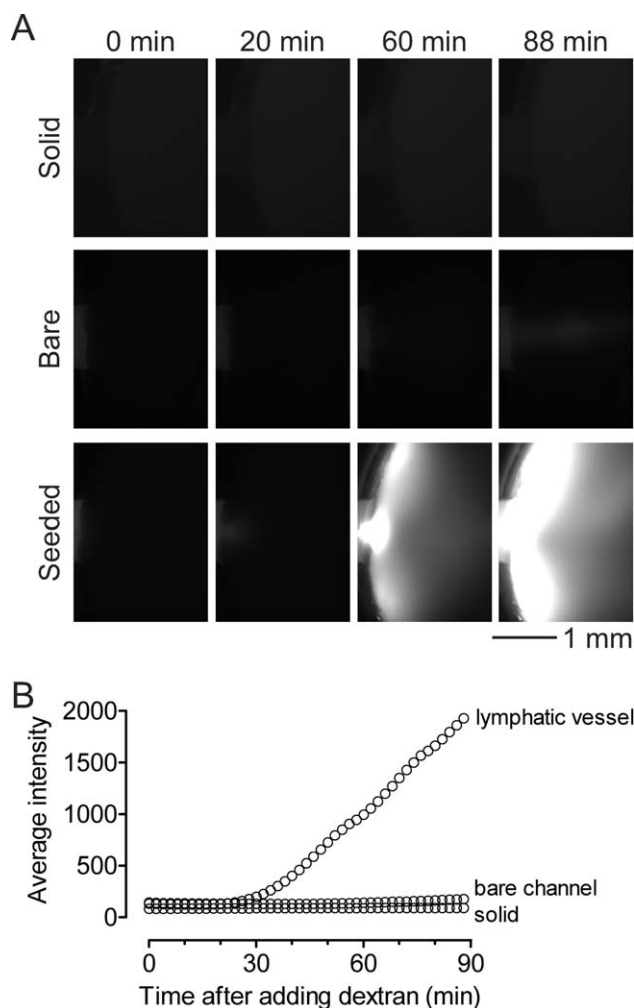


FIGURE 3. Drainage of fluorescent 10 kDa dextran through 19-mm-long gels. **A:** Time-lapse fluorescence images at the ends of a solid gel, a gel that contained a bare channel, and a gel that contained a lymphatic vessel. Shown are images at 0, 20, 40, 60, and 88 min after introduction of solute. In all images, solute was added from the left side. **B:** Plots of fluorescence intensity (averaged over the ROI) versus time for the three gels.

difference of ~ 0.4 cm H_2O for at least 4 h. Media that contained fluorescently labeled dextran and/or BSA was then added to the solid end of scaffolds under the same reverse pressure difference. The resulting fluid drainage and solute convection led to transport of solute through the solid portion of the gel, and then through the lumen of the vessel or channel, before solute escaped through the open end of the vessel or channel.

Time-lapse images of the drainage of fluorescent 10 kDa dextran in solid gels, gels that contained a bare drainage channel, and gels that contained a lymphatic vessel showed characteristic drainage patterns [Fig. 3(A)]. The imaging window was located at the end opposite to the site of solute addition [i.e., at the red dotted region in Fig. 1(A)]. Little fluorescence signal was detected in solid gels throughout the entire imaging period. In gels that contained a bare channel or a lymphatic vessel, fluorescence was visible near

the outlet of the channel nearly 60 or 30 min after solute was added, respectively. The fluorescence intensities increased over time [Fig. 3(B)].

Quantitative measurements of drainage rates were calculated from time-lapse fluorescence intensity data by taking the slope (typically, of the last 20 min) of the intensity versus time curve and normalizing by the exposure time and the intensity of the bulk solute-containing media. Intensity normalization was required to enable quantitative comparison of drainage rates that were obtained using different fluorophores. The three representative intensity-time plots in Figure 3(B) yielded drainage rates of $2.42 \times 10^{-7}/\text{min}$ for a solid gel, $1.85 \times 10^{-5}/\text{min}$ for a gel that contained a bare channel, and $4.04 \times 10^{-4}/\text{min}$ for a gel that contained a lymphatic vessel, respectively.

We found that several solid gels displayed negative drainage rates. These negative values were most likely the result of photobleaching, as crosslinking of collagen by genipin led to gel autofluorescence [visible as faint signal on the left sides of images in Fig. 3(A)]. To determine the sensitivity of the drainage assay, we repeated the calculations on samples in the absence of fluorescent solute, which should have a zero drainage rate in the absence of autofluorescence. Because these control experiments yielded negative drainage rates on the order of $-10^{-6}/\text{min}$, we viewed the assay sensitivity as $10^{-6}/\text{min}$ and set this value as the minimum detectable drainage rate. All solid 19-mm-long gels had nominal drainage rates for 10 kDa dextran of $10^{-6}/\text{min}$.

Gels that contained bare channels drained 10 kDa dextran faster than solid gels did ($9.3^{+9.7}_{-4.7} \times 10^{-5}/\text{min}$; $p = 0.0005$). Seeded channels drained solute at $4.6^{+1.9}_{-1.4} \times 10^{-4}/\text{min}$, a rate that was higher than for solid gels ($p = 0.0001$) and for bare channels ($p = 0.0001$). Thus, although endothelialization had no effect on fluid drainage in 19-mm-long gels, it increased drainage of 10 kDa dextran.

Enhancement of solute drainage by gel length and solute size

To better understand the factors that influence solute drainage, we applied the drainage assay to gels of various lengths and with solutes of various molecular size; five combinations of gel length and solute size were used. These five combinations consisted of the 19-mm-long (“standard”) gels with 10 kDa dextran described above, plus: (i) 9-mm-long (“short”) gels with 10 kDa dextran, (ii) 26-mm-long (“long”) gels with 10 kDa dextran, (iii) standard gels with 3 kDa dextran, and (iv) standard gels with BSA. For each combination, the drainage rates for solid gels and gels that contained bare or seeded channels were measured, for a total of 15 experimental conditions. These drainage data were obtained and analyzed as a cohort, with 33 pairwise comparisons, leading to a Bonferroni-adjusted condition for statistical significance of $p < 0.0015$.

As expected, all gels that contained drainage channels, whether seeded or bare, drained 10 kDa dextran faster than corresponding solid gels of the same length did (p ranging from 0.0001 to 0.0009). Short gels that contained bare or seeded channels drained at similar rates ($p = 0.40$)

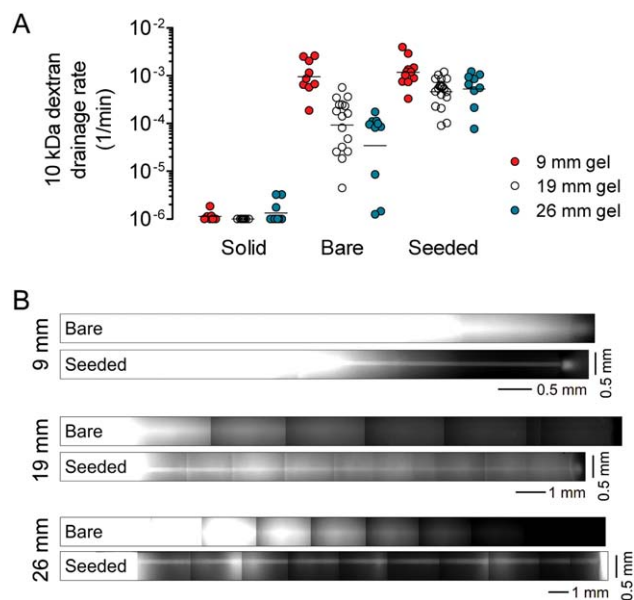


FIGURE 4. Drainage of 10 kDa dextran in gels of different lengths (9, 19, and 26 mm). A: Drainage rates. B: Whole-scaffold fluorescence images after 88 min of drainage in gels that contained bare or seeded channels. In all images, solute was added from the left side. For ease of visualization, gels of different lengths have different axial scaling.

[Fig. 4(A)]. In contrast, long gels that contained a lymphatic vessel drained 10 kDa dextran more quickly than those that were unseeded ($p = 0.0010$). These results suggest that the presence of endothelium increases solute drainage in scaffolds of length ≥ 19 mm; for shorter scaffolds, endothelialization neither increased nor decreased drainage rates.

Whole-scaffold imaging of bare channels showed that 10 kDa dextran tended to diffuse outward from standard or long channels into the surrounding gel, leaving little solute to escape downstream out the mouth of the channel [Fig. 4(B)]. In the corresponding seeded gels, a larger fraction of dextran was retained in the lumen, and the lumen was clearly outlined by fluorescence; where the solute exited at the open ends, local accumulation of solute was observed [Fig. 4(B)]. In short gels, 10 kDa dextran was able to drain through bare channels.

These findings for scaffolds of different lengths suggest that dextran drainage rates should depend strongly on scaffold length for gels that contained bare channels, but less so for those with lymphatic vessels. Indeed, bare channels drained dextran from short scaffolds more rapidly than from standard and long scaffolds ($p = 0.0002$ for short vs. standard, $p < 0.0001$ for short vs. long), with a ~ 27 -fold difference in drainage rates of short and long channels. In contrast, only a ~ 4 -fold difference in drainage rates was detected in short and long vessel-containing gels.

To further shed light on how endothelialization affected solute drainage, we investigated the drainage of 3 kDa dextran and BSA (66 kDa) in 19-mm-long gels. For a given solute, gels that contained channels drained faster than solid gels did (p ranging from <0.0001 to 0.0003) [Fig. 5(A)]. Endothelialization increased the drainage of 3 kDa dextran

($p < 0.0001$), but had no effect on the drainage of BSA ($p = 0.0074$). Fluorescence images showed that, even when draining through bare channels, some BSA did not diffuse out of the channel, certainly not to the same degree that 10 kDa dextran did [compare “BSA, bare” in Fig. 5(B) to “19 mm, bare” in Fig. 4(B)]. In contrast, 3 kDa dextran diffused out of both bare and seeded channels, though to a lesser degree in seeded vessels. In scaffolds that contained bare channels, BSA drained faster than 3 kDa dextran did ($p < 0.0001$; ~ 11 -fold increase), but did not drain significantly faster than 10 kDa dextran did ($p = 0.018$). In seeded scaffolds, only a ~ 2.5 -fold difference between 3 kDa dextran and BSA drainage rates was found. Taken together, these results further support the idea that lymphatic endothelium can increase solute drainage rate by preventing back-diffusion of solute from the channel into the surrounding gel; the smaller the solute, the larger the diffusion coefficient, and the larger the effect of endothelialization on drainage.

DISCUSSION

This study determined to what extent the presence of a blind-ended channel and an endothelium could promote (or inhibit) fluid and solute drainage in type I collagen gels. Not surprisingly, we found that adding a channel to a gel greatly increased fluid and solute drainage. Less expected was the finding that fluid drainage was indifferent to the presence of endothelium. Moreover, endothelium could increase solute drainage, particularly for small solutes and in long scaffolds. The endothelium appeared to function as an imperfect one-way barrier that readily allowed solute to enter the channel, but limited the ability of the solute to escape back into the scaffold along the channel's length. Thus, engineered lymphatics functioned in part like *in vivo* lymphatics, by draining solutes away from the deposit site and preventing them from diffusing back into surrounding tissue.

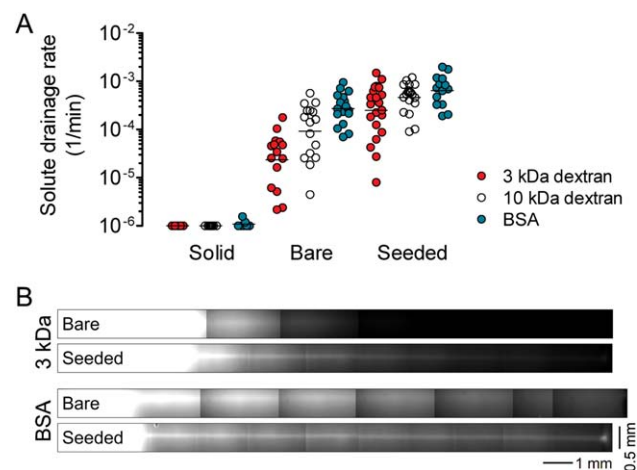


FIGURE 5. Drainage of different solutes (3 kDa dextran, 10 kDa dextran, and BSA) in 19-mm-long gels. A: Drainage rates. Data for 10 kDa dextran (open circles) are reproduced from Figure 4(A). B: Whole-scaffold fluorescence images after 88 min of drainage in gels that contained bare or seeded channels. In all images, solute was added from the left side.

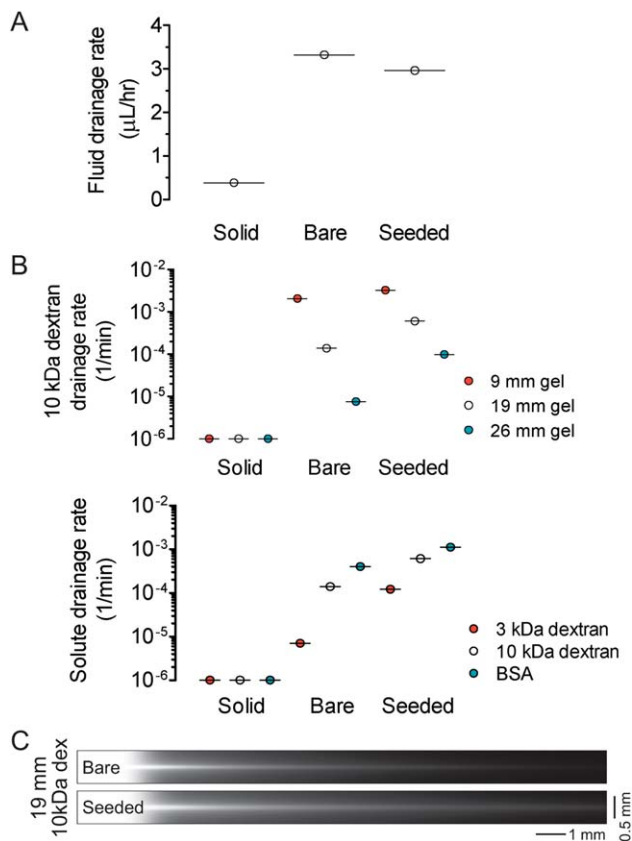


FIGURE 6. Computed fluid and solute drainage rates from finite-element models that incorporate a flow-dependent endothelial hydraulic conductivity. **A:** Plot of computed fluid drainage rates for various gel configurations. This plot is analogous to that in Figure 2(A). **B:** Plots of computed solute drainage rates for various gel configurations and solutes. These plots are analogous to those in Figures 4(A) and 5(A); for consistency of presentation, solute drainage rates below 10^{-6} /min are plotted as 10^{-6} /min. **C:** Computed solute distributions for 10 kDa dextran in a 19-mm-long channel after 88 min of drainage, in scaffolds that contain bare or endothelialized channels. These images are analogous to the ones for 19-mm-long gels in Figure 4(B).

Determinants of solute drainage rates

Why endothelium did not hinder solute drainage is easily rationalized, but it is less obvious how endothelium could enhance drainage. Intuitively, one would expect that an LEC layer, no matter how leaky, would not promote transport beyond the level achieved in cell-free channels. Whole-scaffold images of solute transport [Figs. 4(B) and 5(B)] shed light on possible mechanisms. These images showed that once solute entered a channel, the presence of endothelium helped to determine whether the solute remained confined to the lumen during its transit to the open end of the channel.

This concept can be made more concrete by considering the relevant transport times. In any given drainage channel, the minimum time τ_{channel} required for the solute to traverse the length of channel is roughly L/v , where L is the channel length and v is the centerline flow speed in the channel. In bare channels, the time τ_{bare} required for the solute to diffuse back into the gel is roughly R^2/D , where R is the channel radius and D is the solute diffusion coefficient. If, τ_{channel} is less than τ_{bare} , then solute will drain out of a scaffold before it

noticeably diffuses back into the gel. In this case, adding endothelium would do little to enhance drainage rates. If, τ_{channel} is greater than τ_{bare} , then much of the solute will diffuse out of the channel and will not be available to drain from the scaffold; here, solute will be moved from one part of the scaffold to another, much as is observed in tissues during lymphatic insufficiency *in vivo*.²⁵

When the channel is covered by endothelium, τ_{bare} is augmented by a characteristic time τ_{EC} for transport of solute across the endothelium. Here, τ_{EC} is on the order of R/P_e , where P_e is the endothelial solute permeability. The ratio $\tau_{\text{EC}}/\tau_{\text{bare}}$ controls the relative importance of EC and luminal solute transport resistance. When τ_{channel} is greater than τ_{bare} and when $\tau_{\text{EC}}/\tau_{\text{bare}} > 1$, endothelialization will result in a noticeable increase in solute drainage.

Based on fluid drainage rates of ~ 2 $\mu\text{L/h}$ [Fig. 2(A)], we estimate τ_{channel} to be 70 s, 3 min, and 4 min for 9-, 19-, and 26-mm-long gels, respectively. Published values of solute diffusion coefficients²³ suggest τ_{bare} in 120- μm -diameter channels to be roughly 30, 60, and 80 s for 3 kDa dextran, 10 kDa dextran, and BSA, respectively. Thus, τ_{channel} is much greater than τ_{bare} for 19- and 26-mm-long gels, but not for 9-mm-long ones. Typical 10 kDa dextran and BSA permeabilities for vessels under lymphatic-like flows are on the order of 5×10^{-6} cm/s,²⁶ yielding τ_{EC} on the order of 20 min; 3 kDa dextran should have smaller τ_{EC} . Altogether, these values are consistent with the finding that endothelialization enhanced solute drainage in ≥ 19 -mm-long gels, with larger increases for drainage rates of smaller solutes. In contrast, τ_{channel} is comparable to τ_{bare} in 9-mm-long gels, which explains why bare channels and vessels drained solutes at similar rates in these scaffolds. These calculations also explain our finding that solute drainage through bare channels was more sensitive to gel length and solute size than drainage through vessels was.

Computational models of drainage

To further assess these ideas, we constructed finite-element models of fluid and solute transport in the gel configurations that were studied experimentally. In gels that contain lymphatic vessels, the endothelial hydraulic conductivity was taken to be a log-linear function of transmural fluid flow, as shown in Figure 2(B). These models demonstrated that endothelialization decreases fluid drainage rate in 19-mm-long gels by a small amount (11%) that was comparable to the statistically insignificant $\sim 7\%$ decrease found experimentally [Fig. 6(A)]. The dependence of solute drainage rates on gel length, the presence of a channel with and without seeding, and solute size showed a remarkable likeness to that found experimentally [Fig. 6(B)]. Moreover, these models showed that the endothelial hydraulic conductivity was highest at the vessel tips ($\sim 10^{-4}$ cm³/dyn-s), and decayed rapidly to a baseline value ($\sim 10^{-6}$ cm³/dyn-s) at regions located ≥ 1 mm away from the tip. The leakiness of the endothelium at the vessel tips is consistent with the experimental finding that fluid drainage rates were largely independent of endothelialization; apparently, the endothelium at the vessel tip is so leaky that it does not provide

any appreciable barrier to fluid (and solute) influx. Whole-channel views of computed solute distribution at the last time-point [Fig. 6(C)] displayed similar characteristics to experimental distributions [“19 mm, bare” and “19 mm, seeded” in Fig. 4(B)]; solute escaped from bare channels, but to a much lesser extent from vessels, into the surrounding scaffold. The ability of computational models that are based on a flow-dependent endothelial permeability to reproduce experimental findings both qualitatively and quantitatively suggests that our proposed picture of lymphatic drainage—in which endothelium allows fluid and solute escape at the vessel tip, but not re-entry along the vessel length—is reasonable.

Implications for lymphatic design

Our current study suggests that two dimensionless numbers, $\tau_{\text{bare}}/\tau_{\text{channel}} = vR^2/LD$ and $\tau_{\text{EC}}/\tau_{\text{channel}} = vR/LP_e$, would be useful for designing efficient drainage systems for engineered tissues. The higher these ratios, the greater the solute drainage that a channel provides. At first glance, these expressions appear to imply that one should make the drainage channel as wide as possible to maximize the efficacy of drainage. A trade-off exists, however, between ease of drainage and the fraction of the scaffold that is occupied by the channel²⁷; a wide drainage channel will drain the scaffold quickly but will occupy a large volume, decreasing the fraction of the scaffold that is not devoted to drainage. Lining the channel with lymphatic endothelium (or, in principle, any other cell type that displays flow-dependent hydraulic conductivity) has the potential advantage of maintaining high solute drainage rates without increasing the channel volume fraction, and this capability may provide some flexibility in scaffold design to achieve a desired drainage rate.

CONCLUSIONS

Thick tissues will most likely require an explicit drainage system to obtain proper fluid and solute balance. Our current work shows that adding a channel increases fluid and solute drainage rates several-fold. Whether these drainage channels need to be endothelialized to achieve a desired solute drainage rate will depend on the main solute to be drained, the length of the channels, and the fluid drainage rate. *In vivo* lymphoscintigraphy has yielded macromolecular drainage rates on the order of 10^{-4} – 10^{-3} /min, which are comparable to the values we have obtained here with collagen gels.²¹

The method of forming lymphatics in patterned gels is faster than methods that rely on lymphatic vessel sprouting,^{28,29} self-organization of LECs into tubes,³⁰ or interstitial flow-induced lymphatic growth.³¹ In preformed channels, a fully confluent lymphatic vessel can be grown in three days; methods that require lymphatic cells to create their own channels through sprouting or self-organization require much longer times, typically on the order of weeks. The ability to create functional lymphatics in large tissues on a small timescale, using the design principles identified in this study, will be useful for creating implantable tissues with integrated perfusion

and drainage networks and physiological levels of fluid and solute transport.

ACKNOWLEDGMENTS

The authors thank Henry Li for helpful suggestions.

REFERENCES

- Schmid-Schönbein GW. Microlymphatics and lymph flow. *Physiol Rev* 1990;70:987–1028.
- Radhakrishnan K, Rockson SG. The clinical spectrum of lymphatic disease. *Ann NY Acad Sci* 2008;1131:155–184.
- Clayton JM, Hayes AC, Barnes RW. Tissue pressure and perfusion in the compartment syndrome. *J Surg Res* 1977;22:333–339.
- Pepper MS, Skobe M. Lymphatic endothelium: morphological, molecular and functional properties. *J Cell Biol* 2003;163:209–213.
- Leak LV. Structure and function of lymphatic-interstitial interface. In: Staub NC, Hogg JC, Hargens AR, editors. *Interstitial-Lymphatic Liquid and Solute Movement*. Basel: Karger; 1987. p 114.
- Leak LV. Studies on the permeability of lymphatic capillaries. *J Cell Biol* 1971;50:300–323.
- O'Morchoe CCC, O'Morchoe PJ. Differences in lymphatic and blood capillary permeability: ultrastructural-functional correlations. *Lymphology* 1987;20:205–209.
- Baluk P, Fuxe J, Hashizume H, Romano T, Lashnits E, Butz S, Vestweber D, Corada M, Molendini C, Dejana E, McDonald DM. Functionally specialized junctions between endothelial cells of lymphatic vessels. *J Exp Med* 2007;204:2349–2362.
- Lynch PM, Delano FA, Schmid-Schönbein GW. The primary valves in the initial lymphatics during inflammation. *Lymphat Res Biol* 2007;5:3–10.
- Fischer M, Franzeck UK, Herrig I, Costanzo U, Wen S, Schiesser M, Hoffmann U, Bollinger A. Flow velocity of single lymphatic capillaries in human skin. *Am J Physiol* 1996;270:H358–H363.
- Ikomi F, Hunt J, Hanna G, Schmid-Schönbein GW. Interstitial fluid, plasma protein, colloid, and leukocyte uptake into initial lymphatics. *J Appl Physiol* 1996;81:2060–2067.
- Zawieja DC. Contractile physiology of lymphatics. *Lymphat Res Biol* 2009;7:87–96.
- Truslow JG, Price GM, Tien J. Computational design of drainage systems for vascularized scaffolds. *Biomaterials* 2009;30:4435–4443.
- Wong KHK, Truslow JG, Khankhel AH, Chan KLS, Tien J. Artificial lymphatic drainage systems for vascularized microfluidic scaffolds. *J Biomed Mater Res A* 2013;101:2181–2190.
- Price GM, Chrobak KM, Tien J. Effect of cyclic AMP on barrier function of human lymphatic microvascular tubes. *Microvasc Res* 2008;76:46–51.
- Wong KHK, Truslow JG, Khankhel AH, Tien J. Biophysical mechanisms that govern the vascularization of microfluidic scaffolds. In: Brey EM, editor. *Vascularization: Regenerative Medicine and Tissue Engineering*. Boca Raton, FL: CRC Press; 2014. p 109–124.
- Chan KLS, Khankhel AH, Thompson RL, Coisman BJ, Wong KHK, Truslow JG, Tien J. Crosslinking of collagen scaffolds promotes blood and lymphatic vascular stability. *J Biomed Mater Res A* 2014;102:3186–3195.
- Leung AD, Wong KHK, Tien J. Plasma expanders stabilize human microvessels in microfluidic scaffolds. *J Biomed Mater Res A* 2012;100:1815–1822.
- Wong KHK, Truslow JG, Tien J. The role of cyclic AMP in normalizing the function of engineered human blood microvessels in microfluidic collagen gels. *Biomaterials* 2010;31:4706–4714.
- Chrobak KM, Potter DR, Tien J. Formation of perfused, functional microvascular tubes in vitro. *Microvasc Res* 2006;71:185–196.
- Modi S, Stanton AWB, Mortimer PS, Levick JR. Clinical assessment of human lymph flow using removal rate constants of interstitial macromolecules: A critical review of lymphoscintigraphy. *Lymphat Res Biol* 2007;5:183–202.
- Curry FE. Mechanics and thermodynamics of transcapillary exchange. In: Renkin EM, Michel CC, editors. *Handbook of Physiology*; Section 2: The Cardiovascular System. Bethesda, MD: American Physiological Society; 1984. p 309–374.
- Venturoli D, Rippe B. Ficoll and dextran vs. globular proteins as probes for testing glomerular permselectivity: effects of molecular

- size, shape, charge, and deformability. *Am J Physiol Renal Physiol* 2005;288:F605–F613.
24. Michel CC, Curry FE. Microvascular permeability. *Physiol Rev* 1999;79:703–761.
 25. Slavin SA, Upton J, Kaplan WD, Van den Abbeele AD. An investigation of lymphatic function following free-tissue transfer. *Plast Reconstr Surg* 1997;99:730–741. discussion 742–743.
 26. Price GM, Wong KHK, Truslow JG, Leung AD, Acharya C, Tien J. Effect of mechanical factors on the function of engineered human blood microvessels in microfluidic collagen gels. *Biomaterials* 2010;31:6182–6189.
 27. Truslow JG, Tien J. Perfusion systems that minimize vascular volume fraction in engineered tissues. *Biomechanics* 2011;5:022201.
 28. Tammela T, He Y, Lyytikä J, Jeltsch M, Markkanen J, Pajusola K, Ylä-Herttuala S, Alitalo K. Distinct architecture of lymphatic vessels induced by chimeric vascular endothelial growth factor-C/vascular endothelial growth factor heparin-binding domain fusion proteins. *Circ Res* 2007;100:1468–1475.
 29. Choi I, Lee S, Kyoung Chung H, Suk Lee Y, Eui Kim K, Choi D, Park EK, Yang D, Ecoiffier T, Monahan J, Chen W, Aguilar B, Lee HN, Yoo J, Koh CJ, Chen L, Wong AK, Hong Y-K. 9-cis retinoic acid promotes lymphangiogenesis and enhances lymphatic vessel regeneration: Therapeutic implications of 9-cis retinoic acid for secondary lymphedema. *Circulation* 2012;125:872–882.
 30. Hwang JH, Kim IG, Lee JY, Piao S, Lee DS, Lee TS, Ra JC, Lee JY. Therapeutic lymphangiogenesis using stem cell and VEGF-C hydrogel. *Biomaterials* 2011;32:4415–4423.
 31. Goldman J, Conley KA, Raehl A, Bondy DM, Pytowski B, Swartz MA, Rutkowski JM, Jaroch DB, Ongstad EL. Regulation of lymphatic capillary regeneration by interstitial flow in skin. *Am J Physiol Heart Circ Physiol* 2007;292:H2176–H2183.